AIAA JOURNAL
Vol. 42, No. 2, February 2004

Efficient Coupled Zigzag Theory for Hybrid Piezoelectric Beams for Thermoelectric Load

S. Kapuria,* P. C. Dumir,† and A. Ahmed‡
Indian Institute of Technology Delhi, New Delhi 110 016, India

An efficient coupled zigzag theory is developed for electrothermal stress analysis of hybrid piezoelectric beams. The thermal and potential fields are approximated as piecewise linear for the sublayers. The deflection is modeled to account for the transverse normal strain due to piezoelectricity and temperature. The longitudinal displacement is approximated as a combination of third-order global variation and a layerwise linear variation. The shear continuity conditions at the layer interfaces and the shear traction-free conditions at the top and bottom are used to formulate the theory in terms of three primary displacement variables. The theory is assessed by comparing the analytical solution for simply supported beam with the exact piezothermoelasticity solution. Comparisons for two thermal loads on a hybrid test beam devised for this study and hybrid composite beams establish that the present theory yields quite accurate results.

Nomenclature

$A, \bar{A}; A^l, \bar{A}^l$	=	beam stiffness and thermomechanical matrices
a, b, h, L	=	length, width, thickness, number of plys
$D_x, D_z; E_x, E_z$	=	electric displacements and electric field
$d_{ij}, \hat{e}_{ij}$	=	piezoelectric strain and stress constants
F_4^j, G^j, H^j	=	electrical load, resultants of D_z, D_x
$G_{ij}, Y_i, \nu_{ij}, \hat{Q}_{ij}$	=	elastic modulii, Poisson's ratios, reduced stiffnesses
k_0, u_0, ψ_0	=	midsurface layer and its displacement variables
L	=	matrix of differential operators
N_x, M_x, P_x, S_x^j	=	stress resultants of σ_x
$\bar{\boldsymbol{P}}, \bar{\boldsymbol{U}}$	=	load vector, vector of primary variables
$p_3, \hat{p}_3$	=	pyroelectric constants
q_{j_i}	=	extraneous charge density on the actuated surface at $z_\phi^{j_i}$
$R^k, R^{kj}, \bar{R}^{kl}$	=	cubic layerwise functions
S	=	thickness ratio a/h
$u, w; \theta, \phi$	=	displacements and temperature, potential
u_k, ψ_k	=	displacement variables for layer k
$V_x, Q_x, \bar{Q}_x^j, V_\phi^j$	=	stress resultants of τ_{zx}
z_{k-1}	=	z coordinate of bottom of kth layer
$\alpha_i, \hat{\beta}_1$	=	thermal expansion coefficients, stress-temperature coefficient
$\beta^j, \bar{\beta}^j; \beta^{jl}, \bar{\beta}^{jl}$	=	beam electromechanical coupling and electrothermal matrices
$\gamma^{jl}, E^{jj'}, \bar{E}^{jj'}$	=	beam pyroelectric and dielectric matrices
$\eta_{ij}, \hat{\eta}_{ij}$	=	electric permittivities
$\sigma_x, \tau_{zx}; \varepsilon_x, \gamma_{zx}$	=	stresses and strains
$\Psi_\phi^j, \Psi_\theta^l; \bar{\Psi}_\phi^j, \bar{\Psi}_\theta^l$	=	interpolation functions and related integral functions

Received 7 April 2003; revision received 24 September 2003; accepted for publication 24 September 2003.

*Associate Professor, Applied Mechanics Department.
†Professor, Applied Mechanics Department.
‡Graduate Student, Applied Mechanics Department.

I. Introduction

PIEZOELECTRIC hybrid laminates form part of a new generation of adaptive structures. To achieve desired control, their robust coupled thermoelectromechanical models are needed to obtain accurate response. Thermal loading causes significant thermal stresses due to the thermal gradient across the thickness and due to widely different thermal properties of the adjacent layers. Tauchert et al.[1] have presented a review of the work in thermopiezoelasticity for smart structures. Analytical two-dimensional exact piezothermoelasticity solutions[2,3] are available for cylindrical bending of simply supported hybrid panels. The three-dimensional finite element analysis[4] results in a large problem size, which may become computationally costly for practical control problems. Hence, several one-dimensional beam models have been developed. The layerwise material inhomogeneity causes severe layerwise distortion of the normal to the midsurface for moderately thick and thick beams. The classical laminate theory (CLT) and first-order shear deformation (FSDT) theory are inadequate to account for this distortion, and so third-order theory (TOT) and higher-order theories have been developed with the same expansion of displacement across the thickness. In the discrete layerwise theories (DLT), different expansions of displacements are used in various layers with the number of displacement variables dependent on the number of layers. The shear stress continuity conditions at the layer interfaces are violated in the equivalent single-layer theory and DLT. The efficient zigzag theories (ZIGT) are discrete-layer theories in which the primary displacement variables are reduced by using the continuity conditions of shear stress at layer interfaces and shear traction-free conditions at the top and bottom surfaces. In coupled theories, charge equation of equilibrium is included, whereas in the uncoupled theories it is excluded. Elastic beam models[5–7] with induced actuation strain, uncoupled and coupled CLT,[8,9] FSDT,[10–12] TOT,[13–17] DLT,[18,19] and ZIGT[20–23] have been employed for hybrid beams and plates. A new efficient coupled ZIGT is presented here for static thermoelectric stress analysis of hybrid piezoelectric beams, of any layup, by the extension of the ZIGT of Kapuria et al.[22] to the thermal load case. The thermal and electric potential fields are discretized layerwise as piecewise linear for the sublayers. The model considers both the longitudinal and transverse electric fields. The transverse displacement is approximated to account for the transverse normal strain induced by the electric and thermal fields. The longitudinal displacement is approximated as a combination of a global third-order variation across the thickness and a layerwise linear variation. The displacement field is expressed in terms of only three primary displacement variables, a set of electric potential variables, and the thermal field by enforcing exactly the boundary conditions of zero transverse shear stress at the top and bottom and the conditions of

its continuity at the layer interfaces. This theory is as efficient as the coupled first-order theory and TOT. The equilibrium equations and boundary conditions are derived using a variational principle. Analytical Fourier series solutions for this theory are obtained for simply supported hybrid beams and compared with the exact two-dimensional piezothermoelasticity solution. Comparisons for two thermal loads on a hybrid test beam devised for this study and hybrid composite beams establish that the present theory yields quite accurate results.

II. Displacement, Potential, and Temperature Field Approximations

Consider a hybrid beam of width b, thickness h, and length a, made of L perfectly bonded orthotropic layers with longitudinal axis x, subjected to thermal load and with actuation potentials applied to some piezoelectric layers, with no variation along the width. The piezoelectric material, with poling along the thickness axis z, can be of orthorhombic materials of class mm2 symmetry because the commonly used materials lead zirconate titanate (PZT) and polyvinylidene fluoride (PVDF) belong to this class. Let the planes $z = z_0 = -h/2$ and $z = z_L = h/2$ be the bottom and top surfaces of the beam. The z coordinate of the bottom surface of the kth layer (numbered from the bottom) is denoted as z_{k-1}, and its material symmetry direction 1 is at an angle θ_k to the x axis. The reference plane $z = 0$ either passes through or is the bottom surface of the k_0th layer.

The usual assumptions for mathematical simplification of a one-dimensional model that are retained are as follows. Assume $\sigma_y = \tau_{yz} = \tau_{xy} = 0$, $\sigma_z \simeq 0$, and assume the axial and transverse displacements u and w, temperature θ, and electric potential ϕ to be independent of y ($\Rightarrow$ electric field component $E_y = -\phi_{,y} = 0$). The strain–displacement relations and the electric field-potential relations are

$$\varepsilon_x = u_{,x}, \qquad \varepsilon_z = w_{,z}, \qquad \gamma_{zx} = u_{,z} + w_{,x}$$
$$E_x = -\phi_{,x}, \qquad E_z = -\phi_{,z} \tag{1}$$

where a subscript comma denotes differentiation. With these assumptions, the general three-dimensional linear constitutive equations for stresses and electric displacements D_x and D_z yield

$$\sigma_x = \hat{Q}_{11}\varepsilon_x - \hat{e}_{31}E_z - \hat{\beta}_1\theta = \hat{Q}_{11}u_{,x} + \hat{e}_{31}\phi_{,z} - \hat{\beta}_1\theta \tag{2a}$$

$$\tau_{xx} = \hat{Q}_{55}\gamma_{zx} - \hat{e}_{15}E_x = \hat{Q}_{55}(u_{,z} + w_{,x}) + \hat{e}_{15}\phi_{,x} \tag{2b}$$

$$D_x = \hat{e}_{15}\gamma_{zx} + \hat{\eta}_{11}E_x = \hat{e}_{15}(u_{,z} + w_{,x}) - \hat{\eta}_{11}\phi_{,x} \tag{2c}$$

$$D_z = \hat{e}_{31}\varepsilon_x + \hat{\eta}_{33}E_z + \hat{p}_3\theta = \hat{e}_{31}u_{,x} - \hat{\eta}_{33}\phi_{,z} + \hat{p}_3\theta \tag{2d}$$

where $\hat{Q}_{11}$, $\hat{Q}_{55}$, $\hat{e}_{31}$, $\hat{e}_{15}$, $\hat{\eta}_{11}$, $\hat{\eta}_{33}$, $\hat{\beta}_1$, and $\hat{p}_3$ can be expressed in terms of Young's moduli Y_i, shear moduli G_{ij}, Poisson's ratios ν_{ij}, piezoelectric strain constants d_{ij}, electric permittivities η_{ij}, thermal expansion coefficients α_i, and pyroelectric constant p_3.

The potential field is assumed[20] as piecewise linear between n_ϕ points z_ϕ^j, $j = 1, 2, \ldots, n_\phi$, across the thickness h with $z_\phi^1 = z_0$, $z_\phi^{n_\phi} = z_L$, and

$$\phi(x, z) = \Psi_\phi^j(z)\phi^j(x) \tag{3}$$

where $\phi^j(x) = \phi(x, z_\phi^j)$. $\Psi_\phi^j(z)$ are linear interpolation functions for ϕ, and the summation convention is used with the summation index j and the summation index j' (used later), when values $1, 2, \ldots, n_\phi$ are taken. Note that n_ϕ can differ from L and is determined by the required accuracy of ϕ. The thermal problem for the beam can be solved analytically or numerically. For the present theory, θ is approximated as piecewise linear between n_θ points z_θ^l, $l = 1, 2, \ldots, n_\theta$, across the thickness h with $z_\theta^1 = z_0$, $z_\theta^{n_\theta} = z_L$, and

$$\theta(x, z) = \Psi_\theta^l(z)\theta^l(x) \tag{4}$$

where $\theta^l(x) = \theta(x, z_\theta^l)$. $\Psi_\theta^l(z)$ are linear interpolation functions for θ, and the summation convention is used with indices l and l' (used later), when values $1, 2, \ldots, n_\theta$ are taken. Note that n_θ can differ from L and n_ϕ with $n_\theta \geq L$ and is determined by the accuracy required of θ. The choice of the number of points z_θ^l for a layer would depend on the variation of the temperature gradient across its thickness.

Three-dimensional exact solutions[2] have revealed that, for moderately thick hybrid beams under electric potential or thermal load, the deflection w has significant variation across the thickness due to much greater thermoelectric contribution to ε_z compared to the negligible contribution of σ_x. Hence, the deflection w is approximated by integrating the constitutive equation for ε_z by neglecting the contribution of elastic compliance: $w_{,z} \simeq -d_{33}\phi_{,z} + \alpha_3\theta \Rightarrow$

$$w(x, z) = w_0(x) - \bar{\Psi}_\phi^j(z)\phi^j(x) + \bar{\Psi}_\theta^l(z)\theta^l(x) \tag{5}$$

where

$$\bar{\Psi}_\phi^j(z) = \int_0^z d_{33}\Psi_{\phi,z}^j(z)\,\mathrm{d}z$$

is a piecewise linear function and

$$\bar{\Psi}_\theta^l(z) = \int_0^z \alpha_3\Psi_\theta^l(z)\,\mathrm{d}z$$

is a piecewise quadratic function.

The axial displacement for the kth layer is assumed as a combination of a third-order variation across the thickness with layerwise linear variation:

$$u(x, z) = u_k(x) - zw_{0,x}(x) + z\psi_k(x) + z^2\xi(x) + z^3\eta(x) \tag{6}$$

where u_k and ψ_k denote the translation and rotation variables of the kth layer. Substituting ϕ, w, u from Eqs. (3), (5), and (6) into Eq. (2b) yields

$$\tau_{zx} = \hat{Q}_{55}^k\left(\psi_k + 2z\xi + 3z^2\eta\right) + \left[\hat{e}_{15}^k\Psi_\phi^j(z) - \hat{Q}_{55}^k\bar{\Psi}_\phi^j(z)\right]\phi_{,x}^j + \hat{Q}_{55}^k\bar{\Psi}_\theta^l(z)\theta_{,x}^l \tag{7}$$

For the k_0th layer denote $u_0(x) = u_{k_0}(x)$ and $\psi_0(x) = \psi_{k_0}(x)$. The functions u_k, ψ_k, ξ, and η are expressed in terms of u_0 and ψ_0 using the $(L-1)$ conditions each for the continuity of τ_{zx} and u at the layer interfaces and the two shear traction-free conditions $\tau_{zx} = 0$ at the top and the bottom surfaces at $z = z_0, z_L$. The continuity condition of τ_{zx} at interface $z = z_{i-1}$ between layers i and $i-1$ can be expressed in the following recursive form:

$$\begin{aligned}
&\hat{Q}_{55}^i\left[\psi_i + 2z_i\xi + 3z_i^2\eta\right] + \left[\hat{e}_{15}^i\Psi_\phi^j(z_i) - \hat{Q}_{55}^i\bar{\Psi}_\phi^j(z_i)\right]\phi_{,x}^j \\
&\quad + \hat{Q}_{55}^i\bar{\Psi}_\theta^l(z_i)\theta_{,x}^l = \hat{Q}_{55}^{i-1}\left[\psi_{i-1} + 2z_{i-1}\xi + 3z_{i-1}^2\eta\right] \\
&\quad + \left[\hat{e}_{15}^{i-1}\Psi_\phi^j(z_{i-1}) - \hat{Q}_{55}^{i-1}\bar{\Psi}_\phi^j(z_{i-1})\right]\phi_{,x}^j + \hat{Q}_{55}^{i-1}\bar{\Psi}_\theta^l(z_{i-1})\theta_{,x}^l \\
&\quad + 2\hat{Q}_{55}^i(z_i - z_{i-1})\xi + 3\hat{Q}_{55}^i\left(z_i^2 - z_{i-1}^2\right)\eta + \left[\hat{e}_{15}^i\left\{\Psi_\phi^j(z_i)\right.\right. \\
&\quad \left.\left. - \Psi_\phi^j(z_{i-1})\right\} - \hat{Q}_{55}^i\left\{\bar{\Psi}_\phi^j(z_i) - \bar{\Psi}_\phi^j(z_{i-1})\right\}\right]\phi_{,x}^j + \hat{Q}_{55}^i\left[\bar{\Psi}_\theta^l(z_i)\right. \\
&\quad \left. - \bar{\Psi}_\theta^l(z_{i-1})\right]\theta_{,x}^l
\end{aligned} \tag{8}$$

When Eq. (7) is used, $\tau_{zx}(x, z_0) = 0$ is written in the preceding pattern and added to Eqs. (8) for $i = 2, 3, \ldots, k$, to yield

$$\begin{aligned}
&\hat{Q}_{55}^k\left(\psi_k + 2z_k\xi + 3z_k^2\eta\right) + \left[\hat{e}_{15}^k\Psi_\phi^j(z_k) - \hat{Q}_{55}^k\bar{\Psi}_\phi^j(z_k)\right]\phi_{,x}^j \\
&\quad + \hat{Q}_{55}^k\bar{\Psi}_\theta^l(z_k)\theta_{,x}^l = 2C_1^k\xi + 6C_2^k\eta + C_{3j}^k\phi_{,x}^j + C_{4l}^k\theta_{,x}^l \\
&\qquad\qquad\qquad\qquad\qquad\qquad\qquad\qquad\qquad\qquad k = 2, \ldots, L
\end{aligned} \tag{9}$$

where

$$C_1^k = \sum_{i=1}^{k} \hat{Q}_{55}^i (z_i - z_{i-1}), \qquad C_2^k = \sum_{i=1}^{k} \hat{Q}_{55}^i \frac{\left(z_i^2 - z_{i-1}^2\right)}{2}$$

$$C_{3j}^k = \sum_{i=1}^{k} \left\{ \hat{e}_{15}^i \left[\Psi_\phi^j(z_i) - \Psi_\phi^j(z_{i-1}) \right] - \hat{Q}_{55}^i \left[\bar{\Psi}_\phi^j(z_i) - \bar{\Psi}_\phi^j(z_{i-1}) \right] \right\}$$

$$C_{4l}^k = \sum_{i=1}^{k} \hat{Q}_{55}^i \left[\bar{\Psi}_\theta^l(z_i) - \bar{\Psi}_\theta^l(z_{i-1}) \right] \tag{10}$$

With use of Eq. (7), ψ_L is eliminated from the condition $\tau_{zx}(x, z_L) = 0$ and Eq. (9) for $k = L$; using the condition $\tau_{zx}(x, z_0) = 0$ yields

$$2C_1^L \xi + 6C_2^L \eta = -C_{3j}^L \phi_{,x}^j - C_{4l}^L \theta_{,x}^l$$

$$2z_0 \xi + 3z_0^2 \eta = C_5^j \phi_{,x}^j + C_6^l \theta_{,x}^l - \psi_1 \tag{11}$$

where $C_5^j = \bar{\Psi}_\phi^j(z_0) - \hat{e}_{15}^1 \Psi_\phi^j(z_0) / \hat{Q}_{55}^1$, $C_6^l = -\bar{\Psi}_\theta^l(z_0)$. The solution of ξ and η from Eq. (11) is

$$\xi = R_3 \psi_1 + R_5^j \phi_{,x}^j + R_7^l \theta_{,x}^l, \qquad \eta = R_4 \psi_1 + R_6^j \phi_{,x}^j + R_8^l \theta_{,x}^l \tag{12}$$

where

$$R_3 = 4C_2^L / \Delta, \qquad R_4 = -4C_1^L / 3\Delta$$

$$R_5^j = -\left(2z_0^2 C_{3j}^L + 4C_2^L C_5^j\right) / \Delta, \qquad R_6^j = \left(4z_0 C_{3j}^L + 4C_1^L C_5^j\right) / 3\Delta$$

$$R_7^l = -\left(2z_0^2 C_{4l}^L + 4C_2^L C_6^L\right) / \Delta, \qquad R_8^l = \left(4z_0 C_{4l}^L + 4C_1^L C_6^l\right) / 3\Delta \tag{13}$$

with $\Delta = 4z_0^2 C_1^L - 8z_0 C_2^L$. Substituting ξ and η from Eq. (12) into Eq. (9) yields

$$\psi_k = R_2^k \psi_1 + R_{j1}^k \phi_{,x}^j + R_{l2}^k \theta_{,x}^l \tag{14}$$

where

$$R_2^k = a_1^k R_3 + a_2^k R_4$$

$$R_{j1}^k = a_1^k R_5^j + a_2^k R_6^j + \left[C_{3j}^k - \hat{e}_{15}^k \Psi_\phi^j(z_k) \right] / \hat{Q}_{55}^k + \bar{\Psi}_\phi^j(z_k)$$

$$R_{l2}^k = a_1^k R_7^l + a_2^k R_8^l + C_{4l}^k / \hat{Q}_{55}^k - \bar{\Psi}_\theta^l(z_k)$$

$$a_1^k = 2\left(C_1^k / \hat{Q}_{55}^k - z_k\right), \qquad a_2^k = 3\left(2C_2^k / \hat{Q}_{55}^k - z_k^2\right) \tag{15}$$

When Eq. (6) is used, the continuity of u between layers i and $i-1 \Rightarrow u_i + z_{i-1}\psi_i = u_{i-1} + z_{i-1}\psi_{i-1}$, and when Eq. (14) is used,

$$u_i = u_{i-1} + z_{i-1} \left[\left(R_2^{i-1} - R_2^i\right)\psi_1 + \left(R_{j1}^{i-1} - R_{j1}^i\right)\phi_{,x}^j + \left(R_{l2}^{i-1} - R_{l2}^i\right)\theta_{,x}^l \right], \qquad i = 2, \ldots, L \tag{16}$$

Adding Eqs. (16) for $i = 2$–k yields u_k in terms of u_1:

$$u_k = u_1 + \bar{R}_2^k \psi_1 + \bar{R}_{j1}^k \phi_{,x}^j + \bar{R}_{l2}^k \theta_{,x}^l \tag{17}$$

where

$$\bar{R}_2^k = \sum_{i=2}^{k} z_{i-1}\left(R_2^{i-1} - R_2^i\right), \qquad R_{j1}^k = \sum_{i=2}^{k} z_{i-1}\left(R_{j1}^{i-1} - R_{j1}^i\right)$$

$$\bar{R}_{l2}^k = \sum_{i=2}^{k} z_{i-1}\left(R_{l2}^{i-1} - R_{l2}^i\right)$$

Equations (17) and (14) yield, for the k_0th layer,

$$u_0(x,t) = u_{k_0}(x,t) = u_1 + \bar{R}_2^{k_0}\psi_1 + \bar{R}_{j1}^{k_0}\phi_{,x}^j + \bar{R}_{l2}^{k_0}\theta_{,x}^l \tag{18}$$

$$\psi_0(x,t) = \psi_{k_0}(x,t) = R_2^{k_0}\psi_1 + R_{j1}^{k_0}\phi_{,x}^j + R_{l2}^{k_0}\theta_{,x}^l \tag{19}$$

Substituting ξ and η from Eq. (12), u_k from Eq. (17) with u_1 from Eq. (18) and ψ_k from Eq. (14) into Eq. (6) yields

$$u(x,z) = u_0(x) - z w_{0,x}(x) + R_k(z)\psi_1(x) + R_{k\phi}^j(z)\phi_{,x}^j + R_{k\theta}^l(z)\theta_{,x}^l \tag{20}$$

where

$$R_k(z) = R_1^k + zR_2^k + z^2 R_3 + z^3 R_4$$

$$R_{k\phi}^j(z) = R_1^{kj} + zR_{j1}^k + z^2 R_5^j + z^3 R_6^j$$

$$R_{k\theta}^l(z) = R_2^{kl} + zR_{l2}^k + z^2 R_7^l + z^3 R_8^l \tag{21}$$

with $R_1^k = \bar{R}_2^k - \bar{R}_2^{k_0}$, $R_1^{kj} = \bar{R}_{j1}^k - \bar{R}_{j1}^{k_0}$, and $R_2^{kl} = \bar{R}_{l2}^k - \bar{R}_{l2}^{k_0}$. Substituting ψ_1 in terms of ψ_0 from Eq. (19) into Eq. (20) yields the expression of u as

$$u(x,z) = u_0(x) - z w_{0,x}(x) + R^k(z)\psi_0(x) + R^{kj}(z)\phi_{,x}^j(x) + \bar{R}^{kl}(z)\theta_{,x}^l(x) \tag{22}$$

where

$$R^k(z) = R_k(z) / R_2^{k_0} = \hat{R}_1^k + z\hat{R}_2^k + z^2\hat{R}_3 + z^3\hat{R}_4$$

$$R^{kj}(z) = R_{k\phi}^j(z) - R_k(z)R_{j1}^{k_0} / R_2^{k_0} = \hat{R}_1^{kj} + z\hat{R}_{j1}^k + z^2\hat{R}_5^j + z^3\hat{R}_6^j$$

$$\bar{R}^{kl}(z) = R_{k\theta}^l(z) - R_k(z)R_{l2}^{k_0} / R_2^{k_0} = \hat{R}_2^{kl} + z\hat{R}_{l2}^k + z^2\hat{R}_7^l + z^3\hat{R}_8^l \tag{23}$$

with

$$\left(R_1^k,\ \hat{R}_2^k, \hat{R}_3, \hat{R}_4\right) = \left(R_1^k, R_2^k, R_3, R_4\right) / R_2^{k_0}$$

$$\hat{R}_1^{kj} = R_1^{kj} - \hat{R}_1^k R_{j1}^{k_0}, \qquad \hat{R}_2^{kl} = R_2^{kl} - \hat{R}_1^k R_{l2}^{k_0}$$

$$\hat{R}_{j1}^k = R_{j1}^k - \hat{R}_2^k R_{j1}^{k_0}, \qquad \hat{R}_{l2}^k = R_{l2}^k - \hat{R}_2^k R_{l2}^{k_0}$$

$$\hat{R}_5^j = R_5^j - \hat{R}_3 R_{j1}^{k_0}, \qquad \hat{R}_7^l = R_7^l - \hat{R}_3 R_{l2}^{k_0}$$

$$\hat{R}_6^j = R_6^j - \hat{R}_4 R_{j1}^{k_0}, \qquad \hat{R}_8^l = R_8^l - \hat{R}_4 R_{l2}^{k_0} \tag{24}$$

III. Governing Equations

The equilibrium equations and boundary conditions are derived from variational principle for a piezoelectric continuum[24]:

$$\int_V (-\sigma_{ij}\delta\varepsilon_{ij} - D_i \delta\phi_{,i})\, \mathrm{d}V + \int_\Gamma \left(T_i^n \delta u_i + D_n \delta\phi\right) \mathrm{d}\Gamma - \sum_{i=1}^{\bar{n}_\phi} \int_{A^{j_i}} \left(D_{z_u} - D_{z_l}\right)\delta\phi^{j_i}\, \mathrm{d}A^{j_i} = 0 \tag{25}$$

V and Γ are the volume and surface area of the beam. A^{j_i} is an internal surface $z = z_\phi^{j_i}$, where ϕ^{j_i} is prescribed, and $Dz_l - D_{z_u} = q_{j_i}$ is the extraneous surface charge density on this surface and the subscripts u and l refer to the faces of the interface at $(z_\phi^{j_i})^+$ and $(z_\phi^{j_i})^-$. The total number of such prescribed potentials is $\bar{n}_\phi$. For outward normal $\bar{n} = n_i e_i$, $D_n = D_i n_i$, and stress vector $\boldsymbol{T}_i^n = \sigma_{ji} n_j$. With use of the notation

$$\langle \cdots \rangle = \sum_{k=1}^{L} \int_{z_{k-1}^+}^{z_k^-} (\cdots) b\, \mathrm{d}z$$

the beam stress resultants N_x, M_x, P_x, S_x^j, V_x, Q_x, $\bar{Q}_x^j$, and V_ϕ^j and the beam electric resultants H^j and G^j are defined by

$$\left[N_x,\, M_x,\, P_x,\, S_x^j\right] = \left\langle \sigma_x[1,\, z,\, R^k(z),\, R^{kj}(z)]\right\rangle$$

$$\left[V_x,\, Q_x,\, \bar{Q}_x^j,\, V_\phi^j\right] = \left\langle \tau_{zx}\left[1,\, R_{,z}^k(z),\, R_{,z}^{kj}(z) - \bar{\Psi}_\phi^j(z),\, \bar{\Psi}_\phi^j\right]\right\rangle$$

$$H^j = \left\langle \Psi_\phi^j(z) D_x\right\rangle, \qquad G^j = \left\langle \Psi_{\phi,z}^j(z) D_z\right\rangle \tag{26}$$

Equations (25) yield coupled equations of equilibrium:

$$N_{x,x} = 0, \qquad M_{x,xx} = 0, \qquad P_{x,x} - Q_x = 0$$

$$-S_{x,xx}^j + \bar{Q}_{x,x}^j + H_{,x}^j - G^j + F_4^j = 0 \tag{27}$$

for $j = 1, 2, \ldots, n_\phi$, with electrical loads $F_4^j = b[D_{z_L}\delta_{jn_\phi} - D_{z_0}\delta_{j1} + q_{j_i}\delta_{jj_i}]$, where δ_{ij} is Kronecker's delta. When prescribed values are denoted by an asterisk, the boundary conditions at the ends at $x = 0, a$ are

$$u_0 = u_0^* \quad \text{or} \quad N_x = N_x^*, \qquad w_0 = w_0^* \quad \text{or} \quad M_{x,x} = V_x^*$$

$$w_{0,x} = w_{0,x}^* \quad \text{or} \quad M_x = M_x^*, \qquad \psi_0 = \psi_0^* \quad \text{or} \quad P_x = P_x^*$$

$$\phi^j = \phi^{j*} \quad \text{or} \quad H^j - S_{x,x}^j + \bar{Q}_x^j = H^{j*} - V_\phi^{j*}$$

$$\phi_{,x}^j = \phi_{,x}^{j*} \quad \text{or} \quad S_x^j = S_x^{j*} \tag{28}$$

When Eqs. (2–5) and (22) are used, the resultants defined by Eq. (26) can be related to u_0, w_0, ψ_0, ϕ^j, and θ^l by

$$\begin{bmatrix} N_x \\ M_x \\ P_x \\ S_x^j \end{bmatrix} = \begin{bmatrix} A_{11} & A_{12} & A_{13} & A_{14}^{j'} \\ A_{12} & A_{22} & A_{23} & A_{24}^{j'} \\ A_{13} & A_{23} & A_{33} & A_{34}^{j'} \\ A_{14}^j & A_{24}^j & A_{34}^j & A_{44}^{jj'} \end{bmatrix} \begin{bmatrix} u_{0,x} \\ -w_{0,xx} \\ \psi_{0,x} \\ \phi_{,x}^{j'} \end{bmatrix} + \begin{bmatrix} \beta_1^{j'} \\ \beta_2^{j'} \\ \beta_3^{j'} \\ \beta_4^{jj'} \end{bmatrix} \phi^{j'}$$

$$+ \begin{bmatrix} A_1^l \\ A_2^l \\ A_3^l \\ A_4^{jl} \end{bmatrix} \theta_{,xx}^l - \begin{bmatrix} \gamma_1^l \\ \gamma_2^l \\ \gamma_3^l \\ \gamma_4^{jl} \end{bmatrix} \theta^l$$

$$\begin{bmatrix} Q_x \\ \bar{Q}_x^j \end{bmatrix} = \begin{bmatrix} \bar{A}_{33} & \bar{A}_{34}^{j'} \\ \bar{A}_{34}^j & \bar{A}_{44}^{jj'} \end{bmatrix} \begin{bmatrix} \psi_0 \\ \phi_{,x}^{j'} \end{bmatrix} + \begin{bmatrix} \bar{\beta}_3^{j'} \\ \bar{\beta}_4^{jj'} \end{bmatrix} \phi_{,x}^{j'} + \begin{bmatrix} \bar{A}_3^l \\ \bar{A}_4^{jl} \end{bmatrix} \theta_{,x}^l$$

$$H^j = \bar{\beta}_3^j \psi_0 + \left(\bar{\beta}_4^{j'j} - \bar{E}^{jj'}\right)\phi_{,x}^{j'} + \bar{\beta}^{jl}\theta_{,x}^l$$

$$G^j = \beta_1^j u_{0,x} - \beta_2^j w_{0,xx} + \beta_3^j \psi_{0,x} + \beta_4^{j'j}\phi_{,xx}^{j'} - E^{jj'}\phi^{j'}$$

$$+ \beta^{jl}\theta_{,xx}^l + \gamma^{jl}\theta^l \tag{29}$$

where the elements of the beam stiffness A and $\bar{A}$, the beam thermomechanical coefficient matrices A^l and $\bar{A}^l$; the beam electromechanical coupling matrices $\beta^{j'}$ and $\bar{\beta}^{j'}$, the beam electrothermal matrices β^{jl} and $\bar{\beta}^{jl}$, the beam pyroelectric matrix γ^{jl}, and the beam dielectric matrices $E^{jj'}$ and $\bar{E}^{jj'}$ are defined in terms of the material constants by

$$\left[A_{11},\, A_{12},\, A_{13},\, A_{14}^{j'},\, A_1^l\right] = \left\langle \hat{Q}_{11}[1,\, z,\, R^k(z),\, R^{kj'}(z),\, \bar{R}^{kl}(z)]\right\rangle$$

$$\left[A_{22},\, A_{23},\, A_{24}^{j'},\, A_2^l\right] = \left\langle \hat{Q}_{11} z[z,\, R^k(z),\, R^{kj'}(z),\, \bar{R}^{kl}(z)]\right\rangle$$

$$\left[A_{33},\, A_{34}^{j'},\, A_3^l\right] = \left\langle \hat{Q}_{11} R^k(z)[R^k(z),\, R^{kj'}(z),\, \bar{R}^{kl}(z)]\right\rangle$$

$$\left[A_{44}^{jj'},\, A_4^{jl}\right] = \left\langle \hat{Q}_{11} R^{kj}(z)[R^{kj'}(z),\, \bar{R}^{kl}(z)]\right\rangle$$

$$\left[\beta_1^{j'},\, \beta_2^{j'},\, \beta_3^{j'},\, \beta_4^{jj'}\right] = \left\langle \hat{e}_{31}\Psi_{\phi,z}^{j'}(z)[1,\, z,\, R^k(z),\, R^{kj}(z)]\right\rangle$$

$$\left[\gamma_1^l,\, \gamma_2^l,\, \gamma_3^l,\, \gamma_4^{jl}\right] = \left\langle \hat{\beta}_1\Psi_\theta^l(z)[1,\, z,\, R^k(z),\, R^{kj}(z)]\right\rangle$$

$$\left[\bar{A}_{33},\, \bar{A}_{34}^{j'},\, \bar{A}_3^l\right] = \left\langle \hat{Q}_{55} R_{,z}^k(z)\left[R_{,z}^k(z),\, R_{,z}^{kj'}(z) - \bar{\Psi}_\phi^{j'}(z),\, \Gamma_k^l(z)\right]\right\rangle$$

$$\left[\bar{A}_{44}^{jj'},\, \bar{A}_4^{jl}\right] = \left\langle \hat{Q}_{55}\left\{R_{,z}^{kj}(z) - \bar{\Psi}_\phi^j(z)\right\}\left[R_{,z}^{kj'}(z) - \bar{\Psi}_\phi^{j'}(z),\, \Gamma_k^l(z)\right]\right\rangle$$

$$\left[\bar{\beta}_3^{j'},\, \bar{\beta}_4^{jj'}\right] = \left\langle \hat{e}_{15}\Psi_\phi^{j'}(z)\left[R_{,z}^k(z),\; R_{,z}^{kj}(z) - \bar{\Psi}_\phi^j(z)\right]\right\rangle$$

$$\gamma^{jl} = \left\langle \hat{p}_3\Psi_{\phi,z}^j(z)\Psi_\theta^l(z)\right\rangle, \qquad E^{jj'} = \left\langle \hat{\eta}_{33}\Psi_{\phi,z}^j(z)\Psi_{\phi,z}^{j'}(z)\right\rangle$$

$$\bar{E}^{jj'} = \left\langle \hat{\eta}_{11}\Psi_\phi^j(z)\Psi_\phi^{j'}(z)\right\rangle \tag{30}$$

The coupled equilibrium equations in terms of the primary variables u_0, w_0, ψ_0, and ϕ^j are obtained by substitution of the expressions of the resultants from Eq. (29) into Eq. (27):

$$L\bar{\boldsymbol{U}} = \bar{\boldsymbol{P}} \tag{31}$$

where $\bar{\boldsymbol{U}} = [u_0\ w_0\ \psi_0\ \phi^1\ \phi^2\ \ldots\ \phi^{n_\phi}]^T$, and $\bar{P} = [P_1\ P_2\ P_3\ P_4^1\ P_4^2\ \ldots P_4^{n_\phi}]^T$. L is a symmetric matrix of linear differential operators in x with

$$L_{11} = -A_{11}()_{,xx}, \qquad L_{12} = A_{12}()_{,xxx}$$

$$L_{13} = -A_{13}()_{,xx}, \qquad L_{1,3+j'} = -A_{14}^{j'}()_{,xxx} - \beta_1^{j'}()_{,x}$$

$$L_{22} = -A_{22}()_{,xxxx}, \qquad L_{23} = A_{23}()_{,xxx}$$

$$L_{2,3+j'} = A_{24}^{j'}()_{,xxxx} + \beta_2^{j'}()_{,xx}, \qquad L_{33} = -A_{33}()_{,xx} + \bar{A}_{33}$$

$$P_1 = A_1^l\theta_{,xxx}^l - \gamma_1^l\theta_{,x}^l, \qquad P_2 = -A_2^l\theta_{,xxxx}^l + \gamma_2^l\theta_{,xx}^l$$

$$L_{3,3+j'} = -A_{34}^{j'}()_{,xxx} + \left[-\beta_3^{j'} + \bar{A}_{34}^{j'} + \bar{\beta}_3^{j'}\right]()_{,x}$$

$$L_{3+j,3+j'} = -A_{44}^{jj'}()_{,xxxx} + \left[-\beta_4^{jj'} - \beta_4^{j'j} + \bar{A}_{44}^{jj'} - \bar{E}^{jj'} + \bar{\beta}_4^{jj'} + \bar{\beta}_4^{j'j}\right]()_{,xx} + E^{jj'}$$

$$P_3 = A_3^l\theta_{,xxx}^l - \gamma_3^l\theta_{,x}^l - \bar{A}_3^l\theta_{,x}^l$$

$$P_4^j = -F_4^j + A_4^{jl}\theta_{,xxxx}^l - \left(\gamma_4^{jl} + \bar{A}_4^{jl} + \bar{\beta}^{jl} - \beta^{jl}\right)\theta_{,xx}^l + \gamma^{jl}\theta^l \tag{32}$$

for $(j, j') = 1, \ldots, n_\phi$. After $\bar{\boldsymbol{U}}$ is solved for, τ_{zx} is obtained by integrating the two-dimensional equation of equilibrium in the x direction.

To assess the coupled ZIGT developed herein, analytical Fourier series solutions are obtained for simply supported beams with the following boundary conditions at $x = 0, a$: $N_x = 0$, $w_0 = 0$, $\phi^j = 0$, $P_x = 0$, $M_x = 0$, and $S_x^j = 0$, for $j = 1, \ldots, n_\phi$. The solutions are compared with the exact piezothermoelastic solution.[2] The details are omitted for brevity.

IV. Results and Assessment

Results are presented for three simply supported hybrid beams a, b, c, which consist of an elastic substrate with a piezoelectric layer of PZT-5A[25] of thickness $0.1h$ bonded to the top. The PZT-5A layer has poling in $+z$ direction. The top and the bottom of the substrate are grounded. The stacking order is mentioned from the bottom. Beam a, which has been devised as a benchmark test case, has a five-ply substrate of thickness $0.09h/0.225h/0.135h/0.18h/0.27h$ of materials 1/2/3/1/3, which have highly inhomogeneous properties for stiffness in tension and shear as in Ref. 26 and highly inhomogeneous coefficients of thermal expansion and thermal conductivities. The orientation $\theta_k = 0$ for all of the plys of beam a. The substrates of beams b and c are made of graphite–epoxy composite of material 4[25] and consist of four plys of equal thickness $0.225h$ with

Table 1 Effect of k^2 on percent error of FSDT for beams with $S = 10$

			k^2			k^2			k^2	
Beam	Load	Entity	5/6	k_w^2	Entity	5/6	k_w^2	Entity	5/6	k_w^2
a	1	$w(0)$	2.62	−3.13	$\sigma_x^e(0.4^-)$	−10.0	−10.0	$\sigma_x^p(0.4^+)$	3.42	3.41
	2	$w(0)$	0.71	−1.85	$\sigma_x^e(0.4^-)$	−6.04	−6.05	$\sigma_x^p(-0.41^+)$	−2.74	−2.74
b	1	$w(0)$	−15.06	−16.98	$\sigma_x^e(0.4^-)$	−3.69	−3.69	$\sigma_x^p(0.5)$	5.20	5.20
	2	$w(0)$	0.21	−1.31	$\sigma_x^e(-0.5)$	−3.95	−3.96	$\sigma_x^p(0.5)$	1.16	1.16
c	1	$w(0)$	−16.7	−14.4	$\sigma_x^e(-0.275^+)$	−4.22	−4.22	$\sigma_x^p(0.5)$	2.67	2.67
	2	$w(0)$	−4.23	−4.83	$\sigma_x^e(0.4^-)$	−1.88	−1.89	$\sigma_x^p(0.4^+)$	1.81	1.81

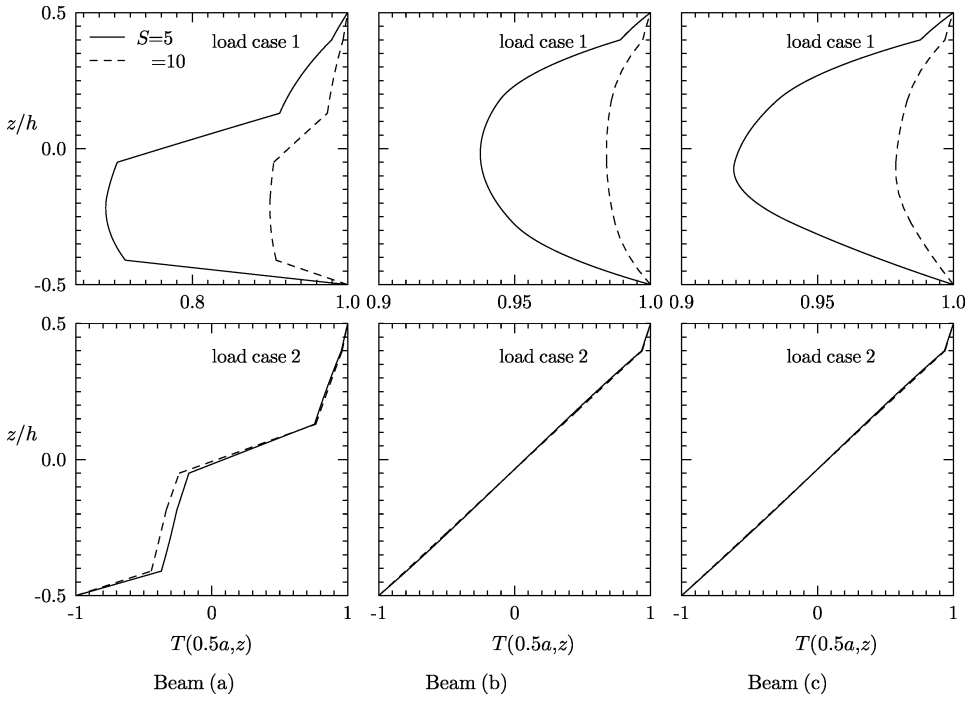

Fig. 1 Temperature distribution for beams a–c under loads cases 1 and 2.

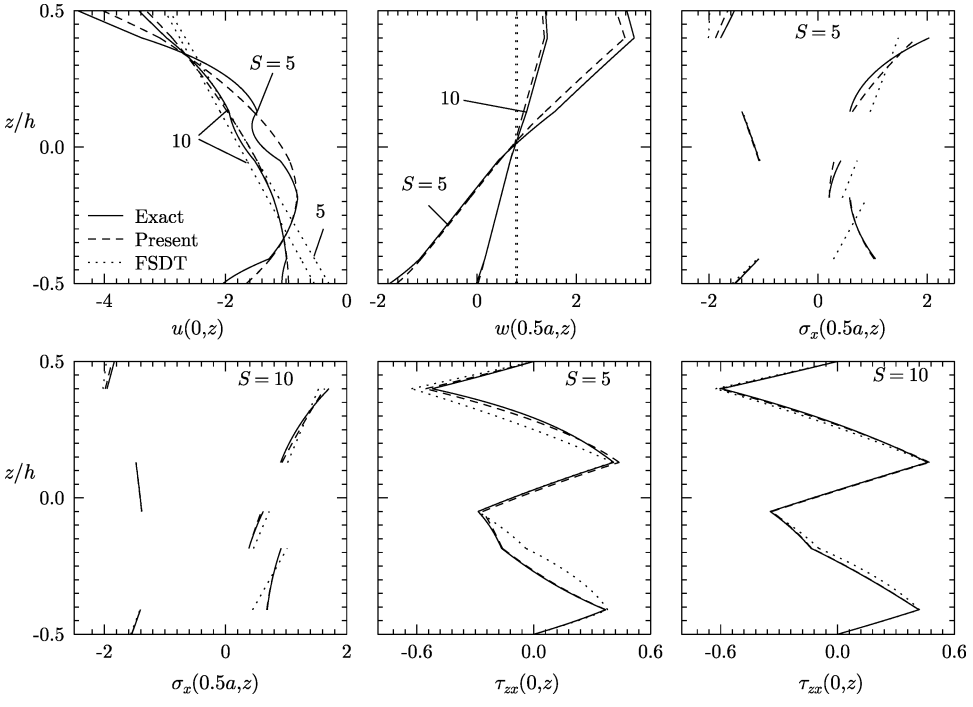

Fig. 2 Distributions of u, w, σ_x, and τ_{zx} for test beam a under load case 1 (open circuit).

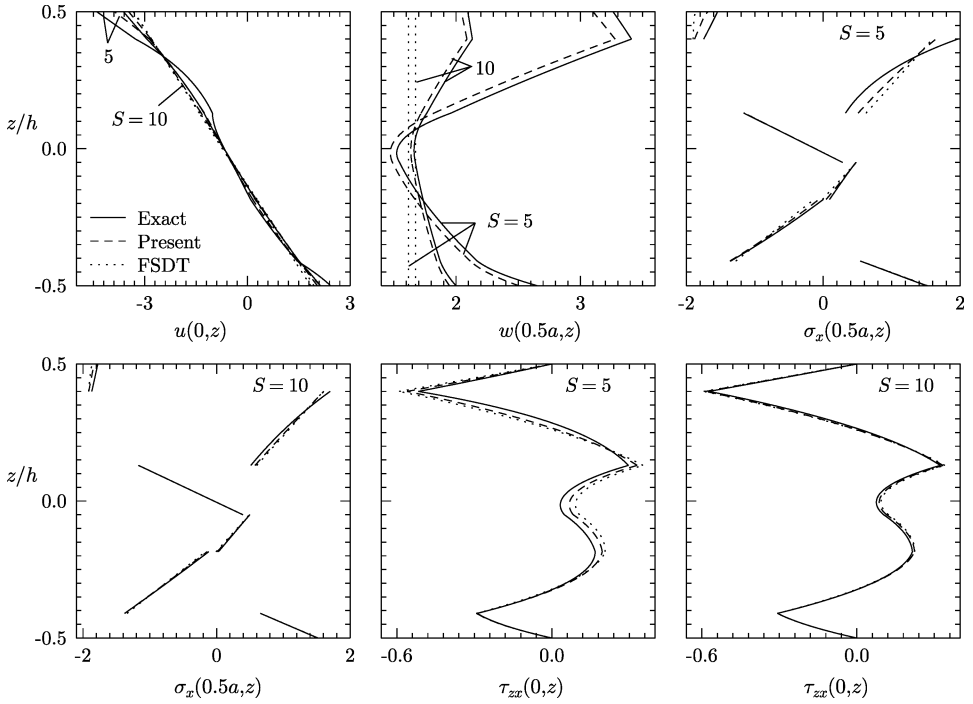

Fig. 3 Distributions of u, w, σ_x, and τ_{zx} for test beam a under load case 2 (open circuit).

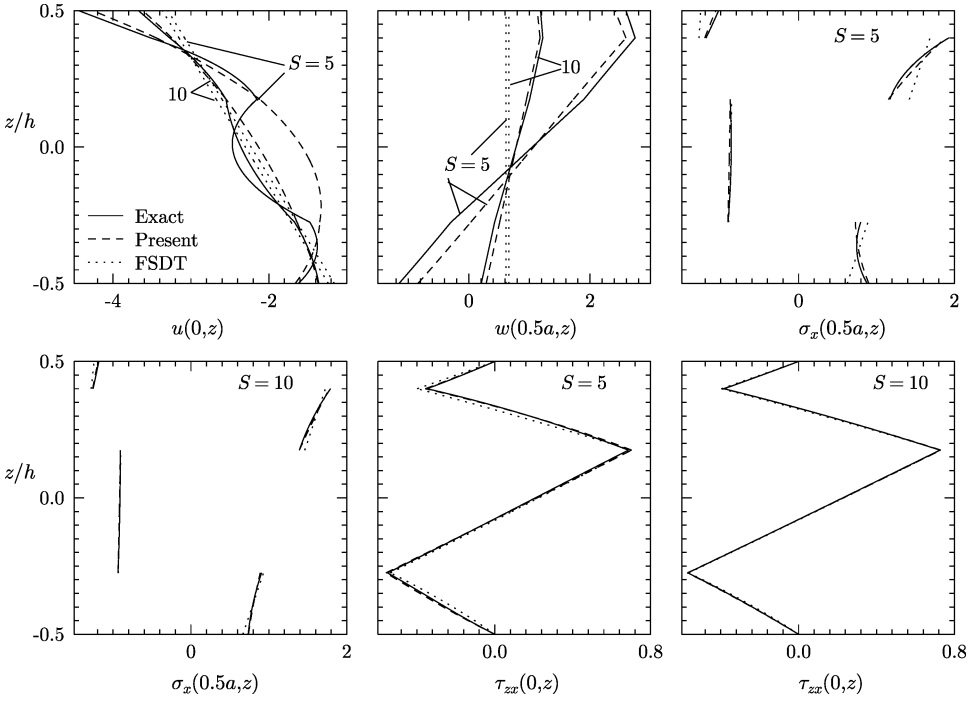

Fig. 4 Distributions of u, w, σ_x, and τ_{zx} for composite beam b under load case 1 (open circuit).

symmetric [0/90/90/0 deg] and antisymmetric [90/0/90/0 deg] layups, respectively. The material properties of materials 1–4 are as follows for Y_L, Y_T, G_{LT}, and G_{TT}; ν_{LT} and ν_{TT}; α_L and α_T; and k_L and k_T. Material 1 is equal to 6.9, 6.9, 1.38, and 1.38 GPa; 0.25 and 0.25; 35.6 and 35.6×10^{-6} K^{-1}; and 0.12 and 0.12 Wm^{-1} K^{-1}. Material 2 is equal to 224.25, 6.9, 56.58, and 1.38 GPa; 0.25 and 0.25; 0.25 and 35.6×10^{-6} K^{-1}; and 7.2 and 1.44 Wm^{-1} K^{-1}. Material 3 is equal to 172.5, 6.9, 3.45, and 1.38 GPa; 0.25 and 0.25; 0.57 and 35.6×10^{-6} K^{-1}; and 1.92 and 0.96 Wm^{-1} K^{-1}. Material 4 is equal to 181, 10.3, 7.17, and 2.87 GPa; 0.28 and 0.33; 0.02 and 22.5×10^{-6} K^{-1}; and 1.5 and 0.5 Wm^{-1} K^{-1}. For PZT-5A the material properties for Y_1, Y_2, Y_3, G_{12}, G_{23}, and G_{31}; and ν_{12}, ν_{13}, and ν_{23} are 61.0, 61.0, 53.2, 22.6, 21.1, and 21.1 GPa; and 0.35, 0.38, and 0.38. Also, d_{31}, d_{32}, d_{33}, d_{15}, and d_{24}; and η_{11}, η_{22}, and η_{33} are equal to -171, -171, 374, 584, and 584×10^{-12} m/V; and 1.53, 1.53, and 1.5×10^{-8} F/m; where α_1, α_2, and α_3; and k_i are equal to 1.5, 1.5, and 2.0×10^{-6} K^{-1}; and 1.8 Wm^{-1} K^{-1}. Here L and T are directions parallel and transverse to the fibres, ν_{LT} is Poisson's ratio for strain in the T direction under uniaxial normal stress in the L direction, and k_L, k_T, and k_i are the thermal conductivity coefficients.

The accuracy of the present theory is assessed by comparison with the exact two-dimensional piezothermoelasticity solution.[2] Because

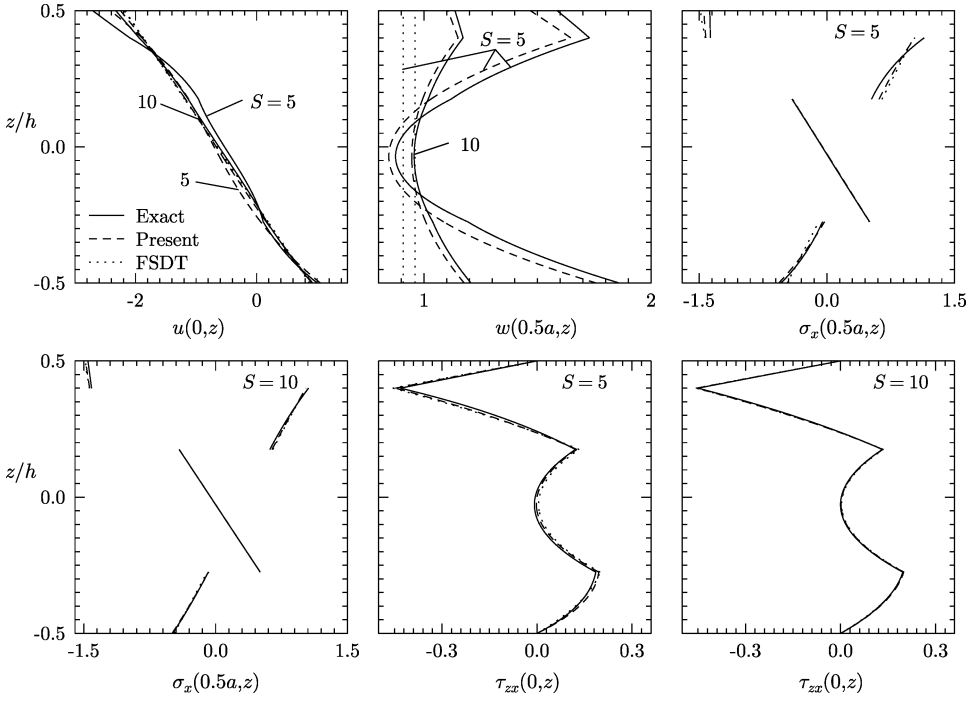

Fig. 5 Distributions of u, w, σ_x, and τ_{zx} for composite beam b under load case 2 (open circuit).

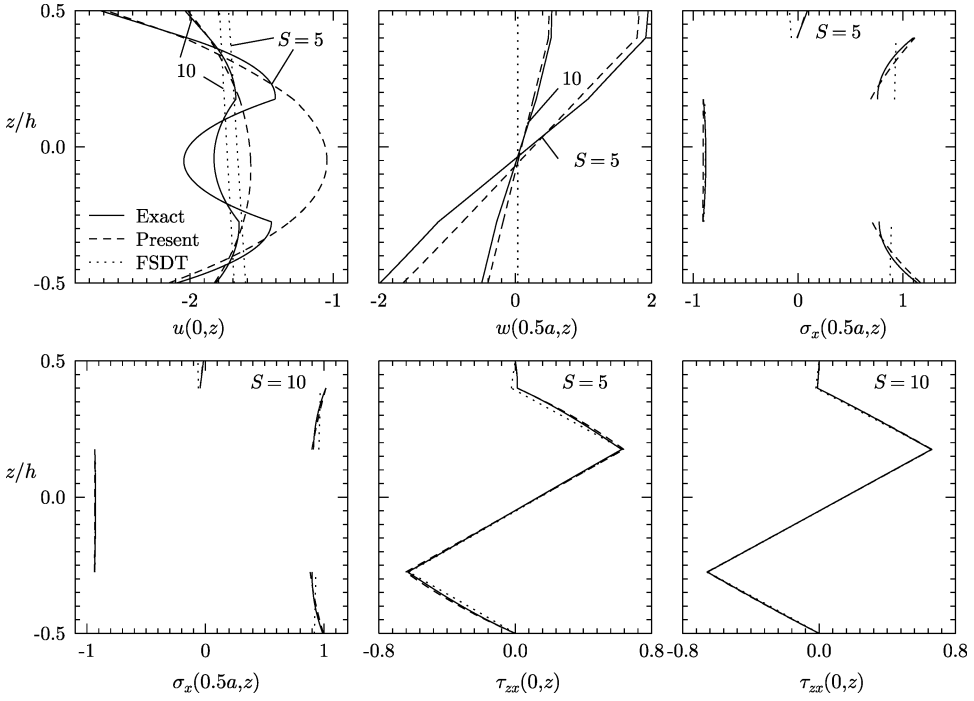

Fig. 6 Distributions of u, w, σ_x, and τ_{zx} for composite beam b under load case 1 (closed circuit).

the number of displacement variables in the present theory is the same as in the FSDT, results are also compared with the FSDT and the existing ZIGT with uniform w across the thickness, which can be obtained from the present ZIGT by setting $\alpha_3 = 0$ and $d_{33} = 0$. No comparison is done with other layerwise theories that involve more displacement unknowns because the accuracy of the present theory is established directly by comparison with the exact solution.

Two load cases considered consist of equal temperature rise at $z = \pm h/2$ and equal temperature rise and fall at $z = \pm h/2$ with sinusoidal longitudinal variation: 1) $\theta(x, \pm h/2) = T_0 \sin(n\pi x/a)$ and 2) $\theta(x, h/2) = -\theta(x, -h/2) = T_0 \sin(n\pi x/a)$.

The results are nondimensionalized as follows with $S = a/h$ and with Y_T, α_T of material 1 for beam a and of material 4 for beams b and c:

$$(\bar{u}, \bar{w}) = 100(u, w/S)/\alpha_T S h T_0, \qquad (\bar{\sigma}_x, \bar{\tau}_{zx}) = (\sigma_x, S\tau_{zx})/\alpha_T Y_T T_0$$

$$\bar{\phi} = \phi d_T/\alpha_T h T_0, \qquad \bar{D}_z = D_z/\alpha_T d_T Y_T T_0, \qquad \bar{T} = T/T_0$$

The overbar is omitted in the following discussion for simplicity. The temperature distributions obtained by the exact two-dimensional analytical thermal solution for the three beams are shown in Fig. 1. Test beam a, devised for this study, is ideal for assessing one-dimensional theories because the temperature profiles are highly nonlinear with large discontinuities in its slope.

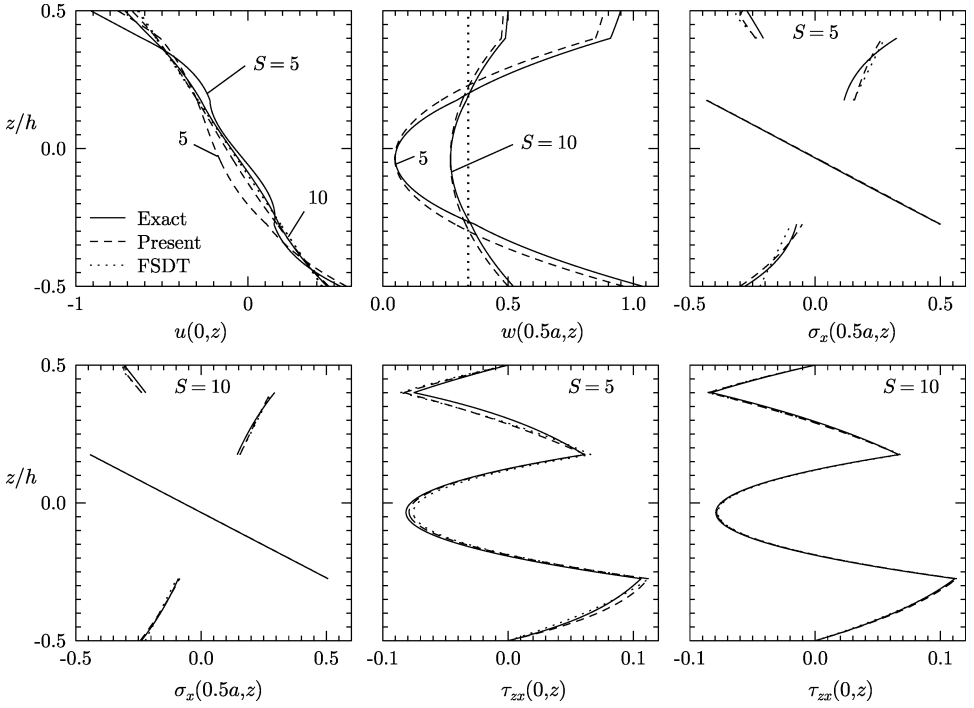

Fig. 7 Distributions of u, w, σ_x, and τ_{zx} for composite beam b under load case 2 (closed circuit).

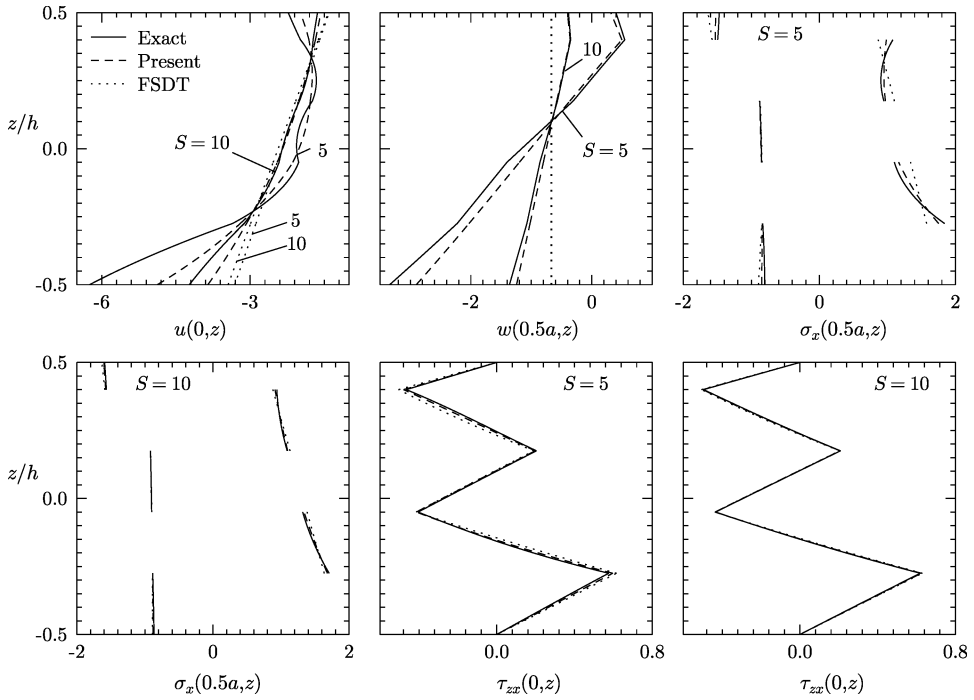

Fig. 8 Distributions of u, w, σ_x, and τ_{zx} for composite beam c under load case 1 (open circuit).

Convergence studies for the ZIGT have revealed that accurate results are obtained by dividing each layer into four equal sublayers for temperature discretization and dividing the piezoelectric layer into four sublayers for potential discretization.

The accuracy of FSDT depends on shear correction factor k^2. The central deflection and the stresses in the elastic and piezolayers where these are large, in the middle cross section, are computed with $k^2 = 5/6$ and with a layup dependent value of k_w^2 according to Whitney's method.[27] The percent errors with respect to the exact two-dimensional solution are compared in Table 1 for beams with $S = 10$. Nondimensional coordinates x/a and z/h are used for tabulating the results. Observe that the stresses for both the thermal loads are not affected by the choice of k^2, but the deflection is a little more accurate for $k^2 = 5/6$ except for beam c under load case 1. A similar trend for these distributions has been found for beams with $S = 5$. Hence, all subsequent results for FSDT have been reported for $k^2 = 5/6$.

The thickness distributions of u and τ_{zx} at the end and of w and σ_{zx} at the center, obtained by the present ZIGT, are compared with the exact two-dimensional thermopiezoelasticity and the coupled FSDT solutions in Figs. 2–9 for beams a, b, and c for the two load cases for open-circuit conditions and also for beam b for the

Table 2 Exact results and percent error of present theory, ZIGT, and FSDT for test beam a (open circuit)

		Load case 1					Load case 2			
S	Entity	Exact	Present	ZIGT	FSDT	Entity	Exact	Present	ZIGT	FSDT
5	$w(0.5, 0.5)$	3.0197	−7.12	−73.3	−73.1	$w(0.5, 0.5)$	3.2618	−4.94	−39.8	−50.4
10		1.3802	−4.94	−43.5	−43.6		2.0943	−2.46	−15.6	−20.0
20		0.91831	−1.97	−16.8	−16.8		1.7967	−0.77	−4.54	−5.87
40		0.79862	−0.58	−4.85	−4.87		1.7220	−0.20	−1.18	−1.53
5	$w(0.5, 0.0)$	0.71438	−3.78	12.9	13.7	$w(0.5, 0.0)$	1.5290	−3.45	28.4	5.86
10		0.75856	−2.10	2.75	2.62		1.6630	−1.58	6.35	0.71
20		0.75926	−0.62	0.68	0.62		1.6893	−0.46	1.53	0.12
40		0.75861	−0.16	0.17	0.15		1.6952	−0.12	0.38	0.02
5	$\sigma_x^e(0.5, 0.4^-)$	2.0375	−11.5	−23.6	−27.8	$\sigma_x^e(0.5, 0.4^-)$	1.9668	−16.3	−14.5	−18.9
10		1.7059	−4.24	−8.75	−10.0		1.7010	−5.59	−4.75	−6.04
20		1.6005	−1.19	−2.48	−2.82		1.6238	−1.53	−1.28	−1.62
40		1.5723	−0.31	−0.64	−0.73		1.6038	−0.39	−0.33	−0.42
5	$\sigma_x^p(0.5, 0.4^+)$	−1.7867	5.23	10.6	12.5	$\sigma_x^e(0.5, -0.41^+)$	−1.3532	0.81	2.19	−5.59
10		−1.9567	1.44	2.97	3.42		−1.3770	−0.07	−0.61	−2.74
20		−2.0097	0.34	0.75	0.86		−1.3717	−0.04	−0.27	−0.82
40		−2.0238	0.06	0.16	0.19		−1.3693	−0.01	−0.08	−0.22
5	$\tau_{zx}(0, 0.4)$	−0.52102	6.57	17.9	20.4	$\sigma_x^p(0.5, 0.4^+)$	−1.7472	7.60	6.86	8.94
10		−0.59563	1.75	4.64	5.18		−1.8685	2.46	2.18	2.68
20		−0.61810	0.44	1.17	1.31		−1.9025	1.00	0.92	1.04
40		−0.62403	0.11	0.29	0.33		−1.9113	0.62	0.60	0.63
5	$10\phi(0.5, 0.5)$	0.53500	0.35	1.03	1.25	$\tau_{zx}(0, 0.4)$	−0.51651	8.57	10.9	14.4
10		0.54392	0.11	0.30	0.36		−0.57281	2.28	2.67	3.49
20		0.54657	0.03	0.08	0.09		−0.58825	0.58	0.66	0.87
40		0.54726	0.01	0.02	0.02		−0.59220	0.15	0.17	0.22
5						$10\phi(0.5, 0.5)$	0.52827	0.45	0.59	0.90
10							0.53381	0.13	0.16	0.24
20							0.53523	0.04	0.04	0.06
40							0.53559	0.01	0.01	0.01

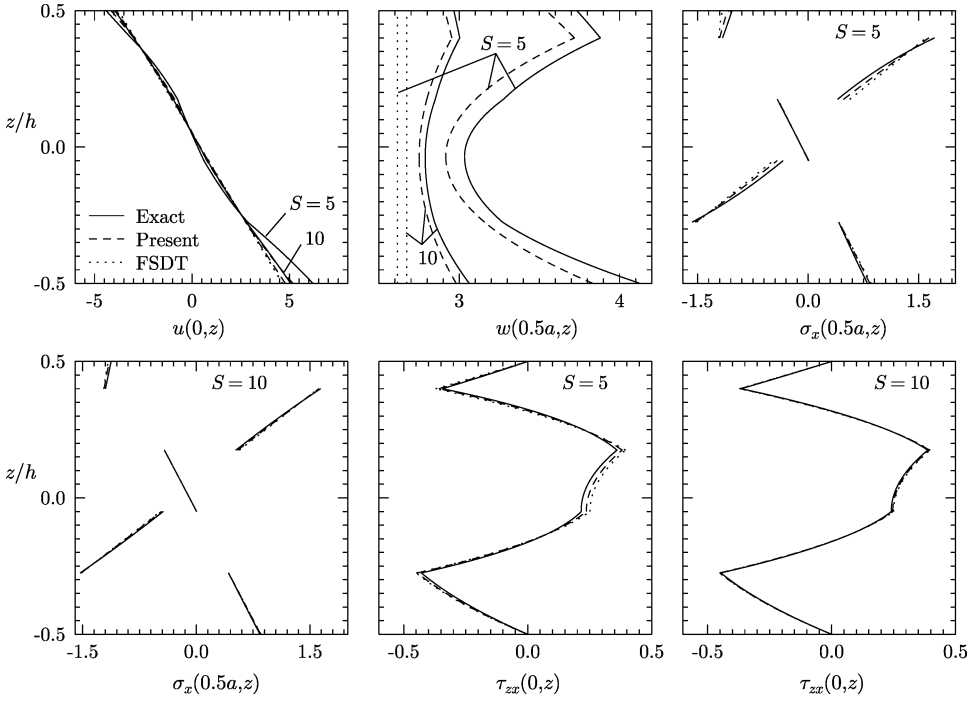

Fig. 9 Distributions of u, w, σ_x, and τ_{zx} for composite beam c under load case 2 (open circuit).

closed-circuit condition. The u distributions of the present ZIGT for load case 2 with the open-circuit condition is in good agreement with the exact two-dimensional solution. For closed-circuit conditions and also for load case 1, the u distributions of the present ZIGT deviate from the two-dimensional solution, especially for the middle layers. It appears from the results that the global quadratic term in u predominates and distorts the local distributions in some layers. The pattern of the distribution of u for the exact solution suggests that the present zigzag model may be improved by replacing the global quadratic term by a local layerwise quadratic term in the approximation of u. This would require a separate study. The FSDT is in most cases unable to approximate the layerwise variation of u. The w distributions for the present ZIGT are in excellent qualitative agreement with the exact two-dimensional solution for all beams with $S = 5$ and 10 for both load cases, with a small quantitative error, whereas the FSDT yields highly erroneous distributions. The σ_x distributions for the present ZIGT closely follow the pattern of the exact two-dimensional solution for all beams in both load

Table 3 Exact results and percent error of present theory, ZIGT, and FSDT for composite beam b (open circuit)

		Load case 1					Load case 2			
S	Entity	Exact	Present	ZIGT	FSDT	Entity	Exact	Present	ZIGT	FSDT
5	$w(0.5, 0.5)$	2.5936	−6.97	−61.4	−76.3	$w(0.5, -0.5)$	1.8609	−5.44	−40.3	−51.2
10		1.1834	−4.54	−35.5	−44.1		1.2072	−2.48	−16.1	−20.4
20		0.80587	−1.74	−13.3	−16.4		1.0360	−0.75	−4.74	−6.01
40		0.70982	−0.50	−3.77	−4.67		0.99266	−0.20	−1.24	−1.58
5	$w(0.5, 0.0)$	1.0469	2.09	−4.19	−41.2	$w(0.5, 0.0)$	0.88154	−3.57	26.0	2.98
10		0.77950	0.08	−2.20	−15.06		0.95844	−1.14	5.67	0.21
20		0.70377	−0.03	0.66	−4.26		0.97355	−0.31	1.37	0.02
40		0.68423	−0.01	−0.18	−1.10		0.97704	−0.08	0.34	0.00
5	$\sigma_x^e(0.5, 0.4^-)$	1.9269	−2.15	−9.23	−12.49	$\sigma_x^e(0.5, 0.4^-)$	1.1425	−9.72	−6.53	−10.9
10		1.7916	−0.81	−2.80	−3.69		1.0570	−2.81	−1.96	−3.15
20		1.7527	−0.22	−0.74	−0.97		1.0337	−0.74	−0.51	−0.82
40		1.7426	−0.06	−0.19	−0.25		1.0277	−0.18	−0.12	−0.20
5	$\sigma_x^e(0.5, 0.175^+)$	1.1732	−1.68	14.0	21.2	$\sigma_x^e(0.5, -0.5)$	−0.53895	5.03	−11.9	−13.3
10		1.3921	−0.05	3.39	4.95		−0.48921	1.21	−3.51	−3.95
20		1.4536	0.01	0.84	1.22		−0.47551	0.29	−0.92	−1.04
40		1.4694	0.01	0.21	0.31		−0.47200	0.07	−0.24	−0.27
5	$\sigma_x^p(0.5, 0.5)$	−1.0272	3.41	16.9	22.2	$\sigma_x^p(0.5, 0.5)$	−1.3765	3.32	3.85	6.89
10		−1.1821	0.96	4.02	5.20		−1.4534	0.30	0.43	1.16
20		−1.2244	0.27	1.02	1.31		−1.4738	−0.47	−0.43	−0.26
40		−1.2353	0.09	0.28	0.35		−1.4790	−0.66	−0.66	−0.61
5	$\tau_{zx}(0, 0.4)$	−0.34764	2.52	10.5	14.5	$\tau_{zx}(0, 0.4)$	−0.43100	3.72	3.48	5.67
10		−0.38292	0.73	2.77	3.55		−0.45005	0.95	0.90	1.43
20		−0.39263	0.19	0.69	0.88		−0.45512	0.24	0.23	0.36
40		−0.39512	0.05	0.17	0.22		−0.45641	0.06	0.06	0.09
5	$10\phi(0.5, 0.5)$	0.53729	0.17	0.79	0.89	$10\phi(0.5, 0.5)$	0.53097	0.22	0.20	0.45
10		0.54324	0.05	0.21	0.24		0.53444	0.06	0.05	0.12
20		0.54483	0.01	0.06	0.06		0.53534	0.01	0.01	0.03
40		0.54524	0.00	0.01	0.01		0.53556	0.00	0.00	0.01

Table 4 Exact results and percent error of present theory, ZIGT, and FSDT for composite beam b (closed circuit)

		Load case 1					Load case 2			
S	Entity	Exact	Present	ZIGT	FSDT	Entity	Exact	Present	ZIGT	FSDT
5	$w(0.5, 0.5)$	1.9491	−6.55	−91.1	−98.1	$w(0.5, 0.5)$	0.94913	−6.94	−68.5	−64.3
10		0.53574	−7.44	−87.2	−93.9		0.49933	−3.57	−33.7	−31.5
20		0.15890	−6.60	−74.5	−80.2		0.38249	−1.20	−11.1	−10.4
40		0.06313	−4.21	−47.0	−50.6		0.35299	−0.34	−3.02	−2.82
5	$\sigma_x^e(0.5, -0.5)$	1.1407	2.63	−25.1	−23.3	$w(0.5, -0.5)$	1.0378	−7.29	−71.3	−67.3
10		0.98918	0.55	−7.72	−7.20		0.52098	−3.99	−36.4	−34.3
20		0.94748	0.13	−2.05	−1.91		0.38787	−1.38	−12.3	−11.6
40		0.93680	0.03	−0.52	−0.49		0.35433	−0.39	−3.39	−3.19
5	$10\sigma_x^p(0.5, 0.4^+)$	−0.11510	−34.3	439	461	$\sigma_x^e(0.5, -0.5)$	−0.28092	6.91	−23.5	−21.40
10		−0.45467	0.05	31.1	32.6		−0.23865	1.83	−7.29	−6.63
20		−0.55348	0.11	6.56	6.87		−0.22736	0.45	−1.95	−1.77
40		−0.57914	0.01	1.55	1.70		−0.22449	0.10	−0.50	−0.46
5	$\tau_{zx}(0, 0.175)$	0.62460	2.03	0.96	1.24	$\sigma_x^p(0.5, 0.5)$	−0.27312	6.22	16.04	14.9
10		0.65922	0.51	0.25	0.32		−0.30746	−1.21	1.06	0.79
20		0.66839	0.13	0.06	0.08		−0.31665	−2.94	−2.38	−2.45
40		0.67072	0.03	0.01	0.02		−0.31898	−3.36	−3.23	−3.24
5	$D_z(0.5, 0.5)$	8.1097	0.10	0.75	0.79	$\tau_{zx}(0, -0.275)$	0.10612	5.05	6.13	5.72
10		8.1775	0.03	0.20	0.21		0.11145	1.27	1.55	1.44
20		8.1957	0.01	0.05	0.05		0.11288	0.30	0.37	0.35
40		8.2004	0.00	0.01	0.01		0.11324	0.06	0.08	0.07
5						$D_z(0.5, 0.5)$	8.0143	0.99	1.07	1.06
10							8.0450	0.82	0.84	0.84
20							8.0529	0.78	0.78	0.78
40							8.0549	0.77	0.77	0.77

cases. The σ_x distributions for FSDT are good for load case 2 but have inaccurate distributions in some outer elastic layers for load case 1 with significant errors. The distributions of postprocessed τ_{zx} obtained by the present ZIGT and the FSDT are very good for all beams with the FSDT having generally larger error. Comparison of the results in Figs. 4 and 5 for beam b with the open-circuit condition and the results in Figs. 6 and 7 for beam b with the closed-circuit condition reveals that the electrical boundary conditions have very large effect on u, w, and σ_x for both load cases and on τ_{zx} for load case 2. A large potential is induced at the top surface due to the presence of pyroelectric coupling, to satisfy the open-circuit condition $D_z = 0$. Consequently, the displacements and stresses in the open-circuit condition are significantly different from those for the closed-circuit condition.

The exact two-dimensional piezothermoelasticity results for displacements, stress, ϕ, and D_z at typical points across the thickness where they are large, along with the percent errors in the present ZIGT (Present), coupled ZIGT and coupled FSDT are given in Tables 2–5 for three beams under two load cases for $S = 5$, 10, 20, and 40. The error in w for the present theory is small for moderately thick beams with the maximum error for $S \geq 10$ at 7.44% for load case 1 and 3.5% for load case 2. The corresponding maximum

Table 5 Exact results and percent error of present theory, ZIGT, and 0FSDT for composite beam c (open circuit)

		Load case 1					Load case 2			
S	Entity	Exact	Present	ZIGT	FSDT	Entity	Exact	Present	ZIGT	FSDT
5	$w(0.5, 0.5)$	0.39938	−21.5	85.2	−268	$w(0.5, 0.5)$	3.7336	−5.10	−16.3	−29.9
10		−0.38573	4.68	76.0	71.4		2.9669	−1.91	−5.51	−9.93
20		−0.58944	0.72	12.5	11.8		2.7614	−0.54	−1.51	−2.71
40		−0.64083	0.16	2.88	2.71		2.7091	−0.14	−0.39	−0.69
5	$w(0.5, -0.5)$	−3.3421	−13.2	−77.9	−79.9	$w(0.5, 0.0)$	3.0402	−3.90	2.83	−14.0
10		−1.3615	−8.62	−50.1	−51.4		2.7901	−1.37	0.47	−4.23
20		−0.83605	−3.57	−20.7	−21.2		2.7170	−0.38	0.10	−1.12
40		−0.70265	−1.07	−6.17	−6.33		2.6980	−0.10	0.02	−0.29
5	$\sigma_x^e(0.5, -0.275^+)$	1.8395	−4.77	−12.8	−14.3	$\sigma_x^e(0.5, 0.4^-)$	1.7145	−4.57	−3.59	−6.59
10		1.7071	−1.52	−3.81	−4.22		1.6403	−1.35	−1.10	−1.88
20		1.6692	−0.41	−1.00	−1.10		1.6193	−0.35	−0.29	−0.49
40		1.6594	−0.10	−0.25	−0.28		1.6139	−0.09	−0.07	−0.12
5	$\sigma_x^p(0.5, 0.5)$	−1.4732	3.10	9.75	11.1	$\sigma_x^p(0.5, 0.4^+)$	−1.1614	3.38	2.94	4.60
10		−1.5926	0.75	2.37	2.67		−1.1994	1.51	1.41	1.81
20		−1.6244	0.17	0.57	0.65		−1.2099	0.98	0.96	1.06
40		−1.6325	0.02	0.12	0.14		−1.2126	0.85	0.84	0.87
5	$\tau_{zx}(0, -0.275)$	0.57569	3.64	6.57	7.04	$\tau_{zx}(0, -0.275)$	−0.42887	3.57	4.42	4.83
10		0.61879	0.93	1.65	1.76		−0.44668	0.92	1.12	1.22
20		0.63047	0.23	0.41	0.44		−0.45140	0.23	0.28	0.31
40		0.63345	0.06	0.10	0.11		−0.45260	0.06	0.07	0.08
5	$10\phi(0.5, 0.5)$	0.54773	0.17	0.48	0.68	$10\phi(0.5, 0.5)$	0.52314	0.22	0.31	0.51
10		0.55344	0.05	0.13	0.18		0.52673	0.06	0.08	0.13
20		0.55495	0.01	0.03	0.05		0.52767	0.02	0.02	0.03
40		0.55533	0.00	0.01	0.01		0.52791	0.00	0.01	0.01

errors in the FSDT for $S \geq 10$ are one order more, that is, 93.9% and 31.5% for load case 1 and 2, respectively. Even for very thin beams with $S = 40$, the errors in w for the FSDT are quite large and one order more than the present theory with 50.6 and 2.82% and 4.21 and 0.34% for load cases 1 and 2 for the FSDT and the present theory, respectively. The maximum errors in the FSDT occur for closed-circuit condition in load case 1. The error in w in ZIGT is generally of the same order as in FSDT for both load cases and much larger than that in the present ZIGT except for a small improvement in only the central deflection in beam a for $S \geq 10$.

A similar comparison of the results for σ_x^e in elastic layers reveals that the error percent for the present theory is much smaller compared to the FSDT for all cases with the errors being even one order less for beam b under load case 1 for the closed-circuit condition and for test beam a under load case 2 for the open-circuit condition. In other cases, the relative reduction in errors for σ_x^e for the present theory is in the range of 60–90% except for a low of 30% for beam c under load case 2. A similar reduction in error in σ_x^p in piezoelectric layer occurs for load case 1 with errors for the present theory being one order less than the FSDT for beam b with the closed-circuit condition and with relative reduction in the range of 60–80% for other cases. However, for load case 2, the error in σ_x^p for the present theory is of the same order as in the FSDT or marginally larger than the FSDT for some cases. The errors in τ_{zx} in the present theory are also much smaller compared to the FSDT except for beam b with the closed-circuit condition, for which the errors themselves are small. The errors in ϕ in the present theory are generally less then half of the errors in the FSDT. The errors in D_z in the present theory for beam b with the closed-circuit condition are less the one-seventh of the error in the FSDT for load case 1 and are of the same order for load case 2. The errors in the stresses in ZIGT for both load cases are either a small improvement or deterioration over those of FSDT. Similarly, the error in ϕ/D_z for ZIGT is generally only a small improvement over that of FSDT.

V. Conclusions

An efficient coupled ZIGT has been developed for hybrid piezoelectric beams under thermoelectric loading. The theory satisfies exactly the conditions on transverse shear stress, includes explicitly the piezoelectric and thermal transverse normal strain in the approximation of deflection, and accounts for the longitudinal electric field. The electric boundary conditions have been found to play a very significant role in the response under thermal load. The present ZIGT has been found in most case to yield much more accurate values of deflection, normal stress, shear stress, electric potential, and electric displacement at specific locations where they are large. The present theory generally yields quite accurate thickness distributions of deflection and stresses for moderately thick beams for both loadings and for both electric boundary conditions. The error in deflection for the coupled FSDT is quite large even for thin beams with $S = 20$. Generally the results for all entities in the existing ZIGT are either marginal improvement or deterioration over those of FSDT. The new coupled ZIGT is much more accurate than the previous ZIGT and yet as efficient as the coupled FSDT because it is formulated in terms of only three primary displacement variables.

Acknowledgments

The first author is grateful to the Department of Science and Technology, Government of India, for providing financial assistance under the Science and Engineering Research Council scheme. The authors are grateful to the reviewer for constructive suggestions.

References

[1]Tauchert, T. R., Ashida, F., Noda, N., and Verijenko, V., "Developments in Thermopiezoelasticity with Relevance to Smart Composite Structures," *Composite Structures*, Vol. 48, 2000, pp. 31–45.

[2]Kapuria, S., Dube, G. P., and Dumir, P. C., "Exact Piezothermoelastic Solution for Simply-Supported Laminated Flat Panel in Cylindrical Bending," *ZAMM*, Vol. 77, 1997, pp. 281–293.

[3]Tauchert, T. R., "Plane Piezothermoelastic Response of a Hybrid Laminate—A Benchmark Problem," *Computers and Structures*, Vol. 39, 1997, pp. 329–336.

[4]Benjeddou, A., "Advances in Piezoelectric Finite Element Modeling of Adaptive Structural Elements: A Survey," *Computers and Structures*, Vol. 76, 2000, pp. 347–363.

[5]Bailey, T., and Hubbard, J. E., "Distributed Piezoelectric-Polymer Active Vibration Control of a Cantilever Beam," *Journal of Guidance, Control, and Dynamics*, Vol. 8, 1985, pp. 605–611.

[6]Chandra, R., and Chopra, I., "Structural Modeling of Composite Beams with Induced-Strain Actuators," *AIAA Journal*, Vol. 31, 1993, pp. 1692–1701.

[7]Robbins, D. H., and Reddy, J. N., "Analysis of Piezoelectrically Actuated Beams Using a Layer-Wise Displacement Theory," *Computers and Structures*, Vol. 41, 1991, pp. 265–279.

[8]Crawley, E. F., and de Luis, J., "Use of Piezoelectric Actuators as Elements of Intelligent Structures," *AIAA Journal*, Vol. 25, No. 10, 1987, pp. 1373–1385.

[9]Tauchert, T. R., "Piezothermoelastic Behavior of a Laminated Plate," *Journal of Thermal Stresses*, Vol. 15, 1992, pp. 25–37.

[10]Jonnalagadda, K. D., Blandford, G. E., and Tauchert, T. R., "Piezothermoelastic Composite Plate Analysis Using First-Order Shear Deformation Theory," *Computers and Structures*, Vol. 51, No. 1, 1994, pp. 79–89.

[11]Blandford, G. E., Tauchert, T. R., and Du, Y., "Self Strained Piezothermoelastic Composite Beam Analysis Using First-Order Shear Deformation Theory," *Composites Part B Engineering*, Vol. 30, 1999, pp. 51–63.

[12]Ishiara, M., and Noda, N., "Piezothermoelastic Analysis of a Cross-Ply Laminate Considering the Effects of Transverse Shear and Coupling," *Journal of Thermal Stresses*, Vol. 23, No. 5, 2000, pp. 441–461.

[13]Jonnalagadda, K. D., Tauchert, T. R., and Blandford, G. E., "High-Order Displacement Formulation for a Piezothermoelastic Laminate," *Mechanics of Electromagnetic Materials and Structures*, AMD-Vol. 161/MD-Vol. 42, American Society of Mechanical Engineers, New York, 1993, pp. 145–159.

[14]Chandrashekhara, K., and Donthireddy, P., "Vibration Suppression of Composite Beams with Piezoelectric Devices Using a Higher Order Theory," *European Journal of Mechanics A/Solids*, Vol. 16, 1997, pp. 709–721.

[15]Shen, H. S., "Postbuckling of Shear Deformable Laminated Plates with Piezoelectric Actuators Under Complex Loading Conditions," *International Journal of Solids and Structures*, Vol. 38, 2001, pp. 7703–7721.

[16]Huang, D., and Sun, B., "Approximate Analytical Solutions of Smart Composite Mindlin Beams," *Journal of Sound and Vibration*, Vol. 244, 2001, pp. 379–394.

[17]Gu, H., Chattopadhyay, A., Li, J., and Zhou, C., "A Higher Order Temperature Theory for Coupled Thermo-Piezoelectro-Mechanical Modeling of Smart Structures," *International Journal of Solids and Structures*, Vol. 37, 2002, pp. 6479–6497.

[18]Tang, Y. Y., Noor, A. K., and Xu, K., "Assessment of Computational Models for Thermoelectroelastic Multilayered Plates," *Computers and Structures*, Vol. 61, 1996, pp. 915–933.

[19]Lee, H.-J., and Saravanos, D. A., "Coupled Layerwise Analysis of Thermopiezoelectric Composite Beams," *AIAA Journal*, Vol. 34, No. 6, 1996, pp. 1231–1237.

[20]Kapuria, S., "An Efficient Coupled Theory for Multi-Layered Beams with Embedded Piezoelectric Sensory and Active Layers," *International Journal of Solids and Structures*, Vol. 38, 2001, pp. 9179–9199.

[21]Kapuria, S., Dumir, P. C., and Ahmed, A., "An Efficient Coupled Layer-Wise Theory for Dynamic Analysis of Piezoelectric Composite Beams," *Journal of Sound and Vibration*, Vol. 261, No. 5, 2003, pp. 927–944.

[22]Kapuria, S., Dumir, P. C., and Ahmed, A., "An Efficient Coupled Layer-Wise Theory for Static Analysis of Piezoelectric Sandwich Beams," *Archive of Applied Mechanics*, Vol. 73, 2003, pp. 147–159.

[23]Kapuria, S., Ahmed, A., and Dumir, P. C., "An Efficient Coupled Zigzag Theory for Harmonic Dynamic Analysis of Piezoelectric Composite and Sandwich Beams with Damping," *Journal of Sound and Vibration* (to be published).

[24]Tiersten, H. F., *Linear Piezoelectric Plate Vibrations*, Plenum, New York, 1969, pp. 25–37, 54, 55.

[25]Xu, K., Noor, A. K., and Tang, Y. Y., "Three-Dimensional Solutions for Coupled Thermoelectroelastic Response of Multilayered Plates," *Computer Methods in Applied Mechanics and Engineering*, Vol. 126, 1995, pp. 355–371.

[26]Averill, R. C., and Yip, Y. C., "Efficient Thick Beam Theory and Finite Element Model with Zigzag Sublaminate Approximation," *AIAA*, Vol. 34, 1996, pp. 1626–1632.

[27]Whitney, J. M., "Shear Correction Factors for Orthotropic Laminates Under Static Load," *Journal of Applied Mechanics*, Vol. 40, 1973, pp. 302–304.

A. Palazotto
Associate Editor